High resolution interrogation of tilted fiber grating SPR sensors from polarization properties measurement

Christophe Caucheteur,[1,*] Yanina Shevchenko,[2] Li-Yang Shao,[2] Marc Wuilpart,[1] and Jacques Albert[2]

[1]*Electromagnetism and Telecom Unit, Université de Mons, 31 Boulevard Dolez, Mons, 7000, Belgium*
[2]*Department of Electronics, Carleton University, 1125 Colonel By Drive, Ottawa, Ontario K1S 5B6, Canada*
**christophe.caucheteur@umons.ac.be*

Abstract: The generation of surface plasmon resonances (SPRs) in gold-coated weakly tilted fiber Bragg gratings (TFBGs) strongly depends on the state of polarization of the core guided light. Recently, it was demonstrated that rotating the linear state of polarization of the guided light by 90° with respect to the grating tilt allows to turn the SPR on and off. In this work, we measure the Jones matrix associated to the TFBG transmission properties in order to be able to analyze different polarization-related parameters (i.e. dependency on wavelength of polarization dependent loss and first Stokes parameter). As they contain the information about the SPR, they can be used as a robust and accurate demodulation technique for refractometry purposes. Unlike other methods reported so far, a tight control of the input state of polarization is not required. The maximum error on refractive index measurement has been determined to be ~1 10^{-5} refractive index unit (RIU), 5 times better than intensity-based measurements on the same sensors.

OCIS codes: (060.2370) Fiber optics sensors; (230.1480) Bragg reflectors.

References and links

1. H. J. Patrick, A. D. Kersey, and F. Bucholtz, "Analysis of the response of long period fiber gratings to external index of refraction," J. Lightwave Technol. **16**(9), 1606–1612 (1998).
2. G. Laffont, and P. Ferdinand, "Tilted short-period fiber-Bragg-grating induced coupling to cladding modes for accurate refractometry," Meas. Sci. Technol. **12**(7), 765–770 (2001).
3. C. Caucheteur, and P. Mégret, "Demodulation technique for weakly tilted fiber Bragg grating refractometer," IEEE Photon. Technol. Lett. **17**(12), 2703–2705 (2005).
4. T. Guo, C. Chen, A. Laronche, and J. Albert, "Power-referenced and temperature-calibrated optical fiber refractometer," IEEE Photon. Technol. Lett. **20**(8), 635–637 (2008).
5. S. Baek, Y. Jeong, and B. Lee, "Characteristics of short-period blazed fiber Bragg gratings for use as macro-bending sensors," Appl. Opt. **41**(4), 631–636 (2002).
6. D. Paladino, A. Cusano, P. Pilla, S. Campopiano, C. Caucheteur, and P. Mégret, "Spectral behavior in nano-coated tilted fiber Bragg gratings: effect of thickness and external refractive index," IEEE Photon. Technol. Lett. **19**(24), 2051–2053 (2007).
7. Y. Y. Shevchenko, and J. Albert, "Plasmon resonances in gold-coated tilted fiber Bragg gratings," Opt. Lett. **32**(3), 211–213 (2007).
8. Y. Y. Shevchenko, C. Chen, M. A. Dakka, and J. Albert, "Polarization-selective grating excitation of plasmons in cylindrical optical fibers," Opt. Lett. **35**(5), 637–639 (2010).
9. B. Špačková, M. Piliarik, P. Kvasnicka, C. Themistos, M. Rajarajan, and J. Homola, "Novel concept of multi-channel fiber optic surface plasmon resonance sensor," Sens. Actuators B Chem. **139**(1), 199–203 (2009).
10. Y.-C. Lu, R. Geng, C. Wang, F. Zhang, C. Liu, T. Ning, and S. Jian, "Polarization effects in tilted fiber Bragg grating refractometers," J. Lightwave Technol. **28**(11), 1677–1684 (2010).
11. C. Caucheteur, S. Bette, R. Garcia, M. Wuilpart, S. Sales, J. Capmany, and P. Mégret, "Influence of the grating parameters on the polarization properties of fiber Bragg gratings," J. Lightwave Technol. **27**(8), 1000–1010 (2009).
12. C. Caucheteur, S. Bette, C. Chen, M. Wuilpart, P. Mégret, and J. Albert, "Tilted fiber Bragg grating refractometer using polarization dependent loss measurement," IEEE Photon. Technol. Lett. **20**(24), 2153–2155 (2008).

#139453 - $15.00 USD Received 9 Dec 2010; revised 10 Jan 2011; accepted 10 Jan 2011; published 13 Jan 2011

13. M. Piliarik, and J. Homola, "Surface plasmon resonance (SPR) sensors: approaching their limits?" Opt. Express **17**(19), 16505–16517 (2009), http://www.opticsinfobase.org/oe/abstract.cfm?URI=oe-17-19-16505.

1. Introduction

Refractometry is used in various areas such as quality control in the food industry, process monitoring or biomedicine. As many applications require minimally invasive refractometers that can be interrogated remotely, fiber grating refractometers have been widely developed during the last years. To measure surrounding refractive index (SRI) changes by monitoring the resonant wavelength of fiber gratings, the guided light has to be brought in contact with the outer boundary of the fiber cladding. In this way, the evanescent field of the optical modes penetrates into the external medium to sense the SRI. Among possible configurations to obtain such a mode distribution, tilted fiber Bragg gratings (TFBGs) seem the most promising solution. Contrary to long period fiber gratings refractometers [1], they provide temperature-insensitive SRI measurements [2–4] and are much less sensitive to bending effects [5]. To further improve their sensing performances, nano-scale coatings have been used to tailor the TFBGs amplitude spectral characteristics or to develop (bio-)chemical sensors based on surface plasmon resonances (SPRs) when functionalized gold overlays are used [6,7].

While reducing the coupling to the backward core mode, the tilt angle enhances the light coupling from the core mode to backward-going cladding modes. Consequently, both a core mode resonance and several tens of cladding mode resonances appear simultaneously in TFBGs transmission spectra [2]. In addition, the tilt angle breaks the cylindrical symmetry of the coupling process relative to the state of polarization (SOP) of the guided core light. As a result, a resonant coupling to a plasmon wave can be achieved: when a TFBG is covered by a nano-scale layer of gold, the cladding modes whose effective refractive index and polarization state are equal or close to those of a plasmon wave transfer energy to it across the metallic surface. A pronounced decrease of these cladding mode resonances appears in the TFBG amplitude spectrum, as reported in [8]. This yields an implementation of SPR-based (bio-) sensors easy to fabricate and to use, which does not require mechanical deformation of the fiber (e.g. etching or polishing) and allows remote sensing in very small volumes.

TFBG amplitude spectra contain a large quantity of data not only in the positions but also in the amplitudes of the fine comb of cladding mode resonances [9]. This information is further enriched by the polarization dependence of (gold-coated) TFBGs [10]. As a result, several ways can be pursued to demodulate the spectrum and retrieve the SPR shift induced by a change of the SRI. Up to now, the focus has been on the measurement of the amplitudes of individual cladding mode resonances relative to the core mode resonance after optimization of the input SOP. Using this technique, accuracy of the order of $5\ 10^{-5}$ refractive index unit (RIU) has been reported [8].

In this work, we use a totally different approach based on the measurement and the analysis of the Jones matrix in transmission (i.e. TFBG transfer function). From this measurement, any linear parameter can be extracted. In our study, we focus on both the polarization dependent loss (PDL) and the first normalized Stokes parameter evolution with wavelength. We demonstrate that these two properties yield an unambiguous signature of the SPR that can be straightforwardly tracked over time. The resulting demodulation technique presents two main advantages in comparison to previous techniques. First, it is robust over polarization instabilities and does not require a tight control of the input state of polarization. Second, it gives an improved accuracy since the maximum error on the determination of the SRI has been measured equal to $\sim 1\ 10^{-5}$ RIU with our technique.

2. Experiments

For the work reported here, 1 cm-long TFBGs were manufactured in hydrogen-loaded single-mode optical fiber using a 248 nm excimer pulsed laser and the phase mask technique. The internal tilt angle was set to 10° to ensure strong coupling to cladding modes with effective

#139453 - $15.00 USD Received 9 Dec 2010; revised 10 Jan 2011; accepted 10 Jan 2011; published 13 Jan 2011

refractive index close to 1.30, which is suited to excite plasmons in aqueous media. A 50 nm gold coating was deposited using a sputtering process in two steps. A first deposition is performed with the fiber placed horizontally above the target and the second one after a rotation of 180° along its axis between the two depositions. As the gold deposition is not perfectly uniform all around the fiber cross-section, the fiber orientation was optimized into the sputtering chamber. In practice the tilt plane was placed parallel to the region of higher gold thickness facing the sputtering source.

As any optical fiber device, TFBGs can be represented by a two-by-two Jones matrix that mathematically describes the propagation of light through them. To obtain such a transfer function, the accuracy and rapidity of the optical vector analyzer CTe from *Luna Technologies* were exploited in our experiments. The latter uses coherent, swept-wavelength interferometry to simultaneously measure the four complex entries of the Jones matrix to characterize the device under test, which yields in an arbitrary Cartesian coordinates system:

$$J_{\mathrm{TFBG}}(\lambda) = \begin{pmatrix} a(\lambda) & b(\lambda) \\ c(\lambda) & d(\lambda) \end{pmatrix} \tag{1}$$

where a, b, c and d are complex coefficients and λ is the wavelength. These coefficients contain all the information about the TFBG transmission properties and in particular those induced by the SPR. In the case of fiber gratings, the polarization eigenmodes correspond to the two polarization states that also provide the minimum and maximum transmitted power (also used to define the PDL). As a consequence, in a Cartesian coordinates system that matches the TFBG eigenmodes (subscripts x and y hereafter), Eq. (1) turns into [11]:

$$J_{\mathrm{TFBG}}(\lambda) = \begin{pmatrix} t_x(\lambda) & 0 \\ 0 & t_y(\lambda) \end{pmatrix} \tag{2}$$

where $t_{x(y)}$ represents the complex transmission coefficient along the $x(y)$ orthogonal polarization mode. Equation (1) or (2) allows to derive any linear parameter that characterizes the TFBG. In the following, we will focus on the amplitude spectra obtained for two specific orthogonal SOPs, the first normalized Stokes parameter s_1 and the PDL evolutions with wavelength. If we consider a linear SOP characterized by the Jones vector $(\cos\theta\ \sin\theta)^{\mathrm{T}}$, the TFBG power spectrum is given by:

$$T_{TFBG}(\lambda) = T_x(\lambda)\cos^2\theta + T_y(\lambda)\sin^2\theta \tag{3}$$

where $T_{x(y)}(\lambda) = |t_{x(y)}(\lambda)|^2$. Hence, Eq. (3) yields the TFBG transmitted spectrum for any desired linear SOP. The corresponding s_1 and PDL evolutions with wavelength are then given by the following relationships [11]:

$$s_1(\lambda) = \frac{T_x(\lambda)\cos^2\theta - T_y(\lambda)\sin^2\theta}{T_x(\lambda)\cos^2\theta + T_y(\lambda)\sin^2\theta} \tag{4}$$

$$PDL(\lambda) = \left| 10\log_{10}\left(\frac{T_x(\lambda)}{T_x(\lambda)}\right)\right| \tag{5}$$

Figure 1 depicts the typical evolutions obtained by Eq. (3) to (5) from the measured Jones matrix of a 10° TFBG immerged in oil. Figure 1a shows the two orthogonal transmitted spectra already reported in [8]: for the black curve, the SOP is optimized to exhibit the classical SPR signature (here at a wavelength around 1550 nm) while the orthogonal state (red curve) maximizes the cladding mode resonances across the whole spectrum. Any other SOP results in an intermediate behavior between these two limits. Figure 1b focuses on the PDL. It

#139453 - $15.00 USD Received 9 Dec 2010; revised 10 Jan 2011; accepted 10 Jan 2011; published 13 Jan 2011

can be seen that the core mode back reflection resonance near 1602 nm does not show significant PDL, confirming that the photo-induced birefringence is very small, probably of the order of 10^{-6}. Hence, the large PDL maxima observed at other wavelengths are not due to a birefringence effect but result from the TFBG coupling core mode light to different families of (vector) cladding modes when its polarization is parallel or perpendicular to the tilt plane. Contrary to the evolution obtained for uncoated TFBGs [12], the local PDL maxima do no longer align on a Gaussian-shape envelope over the whole spectrum: a singular point with a strong decrease of the amplitude (here at a wavelength around 1545 nm) materializes a pronounced difference of behavior between smaller and higher wavelengths. This comes from the differential behavior between the orthogonal spectra displayed in Fig. 1a. The cladding mode resonance wavelengths are quasi similar between both spectra at the left side of the spectrum while there is a significant mismatch between even and odd modes at the right side (the mismatch is decreasing from ~0.55 nm around 1550 nm to ~0.25 nm around 1580 nm). As a result, the PDL presents pairs of closely spaced peaks for wavelengths up to ~1543 nm while they are more resolved at higher wavelengths. Around 1545 nm, since the corresponding cladding mode resonances of both spectra appear at the same wavelength and present a similar amplitude, the PDL is characterized by a single peak that presents a smaller amplitude than its neighbors. Hence, a clear SPR signature appears in the PDL curve at a smaller wavelength (~5 nm of difference in our case) than in the amplitude spectrum. In the following, this unique spectral signature will be tracked as a function of the SRI.

Let us note that the same analysis applies to the s_1 curve depicted in Fig. 1c (here for a linear SOP with θ equal to 45°) that is characterized by alternations between positive and negative peaks except at the SPR.

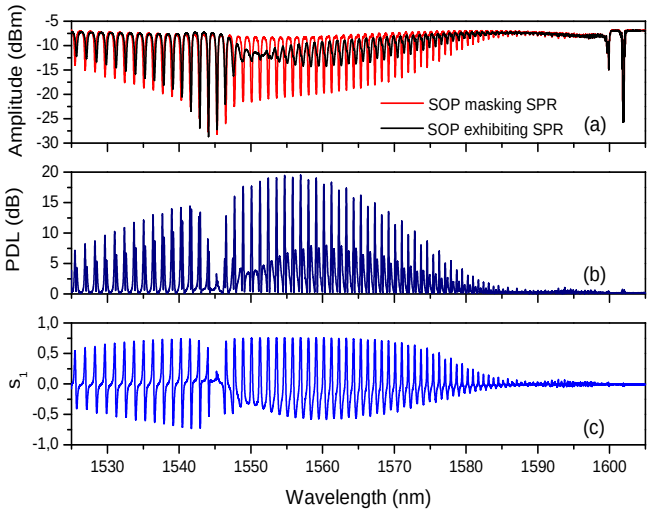

Fig. 1. Orthogonal amplitude spectra (a), PDL (b) and first normalized Stokes evolution (c) for a 10° TFBG immersed in oil.

3. Results and discussion

The proposed demodulation technique based on the analysis of the Jones matrix in transmission was first tested by immersing the gold-coated TFBGs in calibrated refractive index liquids with an accuracy of $2\ 10^{-4}$ that cover a wide range of SRI. Figure 2 and 3 present the evolution of the PDL and s_1 for some SRI values between 1.31 and 1.38. One can see that the SPR signature (marked by an arrow in the graphs) shifts towards longer wavelengths when the SRI increases. As the PDL and s_1 curves are computed from the same raw data, the SPR wavelength is exactly the same for both evolutions. In addition to the wavelength shift, the

#139453 - $15.00 USD Received 9 Dec 2010; revised 10 Jan 2011; accepted 10 Jan 2011; published 13 Jan 2011

amplitude of the single peak corresponding to the SPR signature grows when the SRI increases. This can be attributed to the fact that the SPR resonance becomes wider and less pronounced in the amplitude spectrum for higher SRI values.

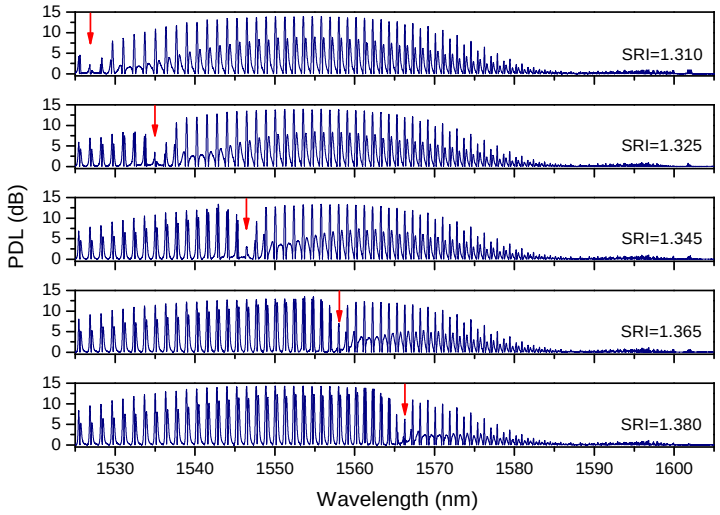

Fig. 2. PDL evolution with wavelength as a function of the SRI.

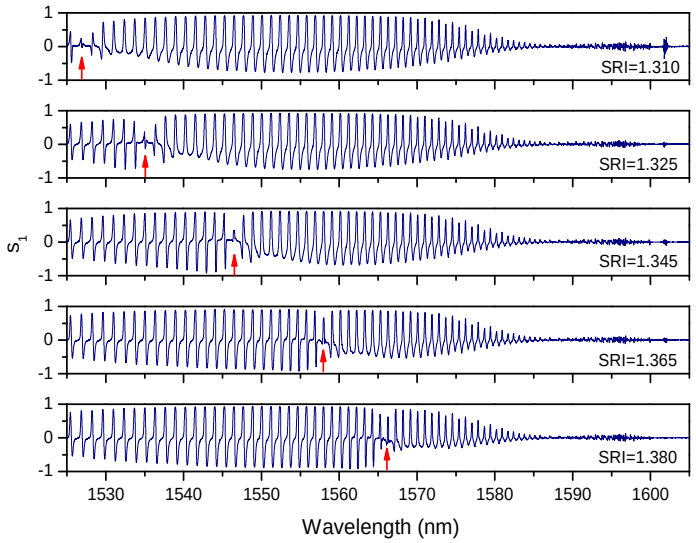

Fig. 3. s_1 evolution with wavelength as a function of the SRI.

To obtain real time measurements, the optical vector analyzer was driven by a program that computes the upper envelope of the PDL (s_1) curve and retrieves its local minimum so as to determine the SPR. Figure 4 displays the result of the upper envelope computation for the PDL curve. Figure 5 presents the SPR wavelength shifts recorded on a wide SRI range. The obtained evolution is linear with a mean sensitivity of 673 nm/RIU, which is standard for the gratings used here. The full width at half-maximum of the envelope is less than 5 nm, much narrower than insertion loss based measurements (including prism-based SPR instruments).

#139453 - $15.00 USD Received 9 Dec 2010; revised 10 Jan 2011; accepted 10 Jan 2011; published 13 Jan 2011

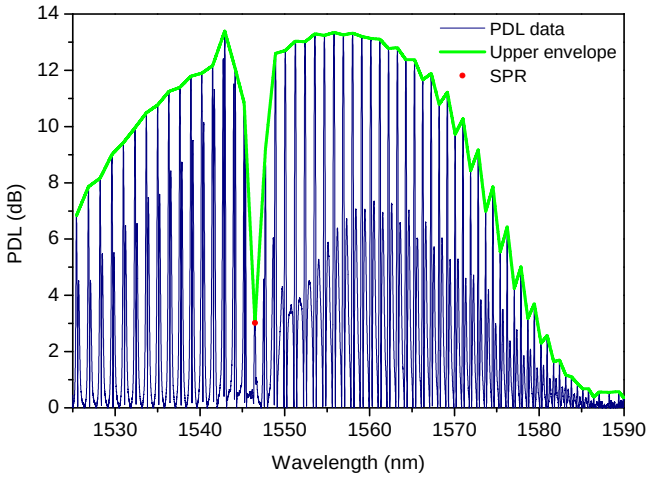

Fig. 4. Computation of the PDL upper envelope.

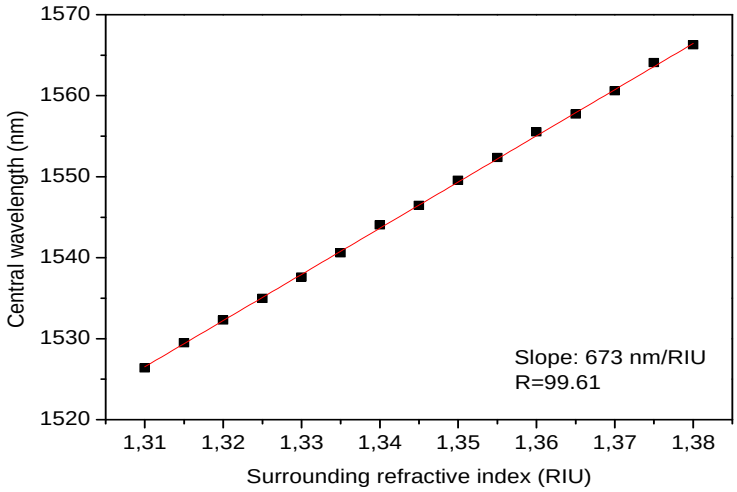

Fig. 5. Shift of the SPR wavelength as a function of the SRI. The straight line is a best fit to the data points.

While Fig. 5 shows that the envelope detection method provides excellent linearity and sensitivity over relatively large SRI ranges, the main application of SPR sensors is to track very small SRI changes, especially in biosensing applications. For such small changes, the accuracy with which the local minimum of the envelope function can be located, while superior to the case of the transmission spectrum, is still insufficient for SPR shifts of the order of a pm. We propose here and demonstrate that the PDL spectrum has narrowband spectral features that possess the necessary sensitivity to small SRI variation. In these experiments, we used a mixture of water and salt (LiCl) to generate controlled refractive index variations. The added volumes were measured with an accuracy of 0.1 ml and the temperature was controlled to 0.1 °C, yielding a nominal refractive index uncertainty of no more than 1.12 10^{-5} RIU. As an example, Fig. 6 presents the evolution of the PDL curve for an SRI range of a few 10^{-5} around 1.34 RIU. Upon close examination, we find that around the SPR signature, some individual peaks of the PDL spectrum shift by amounts that are large in relation to their spectral width (the width of the downward peak of the double-lobed resonance adjacent to the

#139453 - $15.00 USD Received 9 Dec 2010; revised 10 Jan 2011; accepted 10 Jan 2011; published 13 Jan 2011

local SPR in particular, as seen in Fig. 6a). On the other hand, PDL resonances located away from the SPR region towards longer wavelengths, such as the one highlighted in Fig. 6b, do not shift with changing SRI (as expected from low order cladding modes with little field amplitude at the cladding boundary).

We now proceed to show that wavelength shift of a single PDL resonance located near the envelope minimum has a sensitivity to SRI changes that is sufficient to track very small SRI changes. By monitoring the resonance shown in Fig. 6a, we obtain the results of Fig. 7, where the linear regression yields a sensitivity equal to 351 nm/RIU with resonances that have a FWHM of 40 pm (giving a finesse larger than 10^5). The measured sensitivity is close to the theoretical one reported in [9]. The error bars are representative of both the uncertainty on the refractive index value and the accuracy in the wavelength measurement, which is equal to 1.5 pm with the apparatus used in this work.

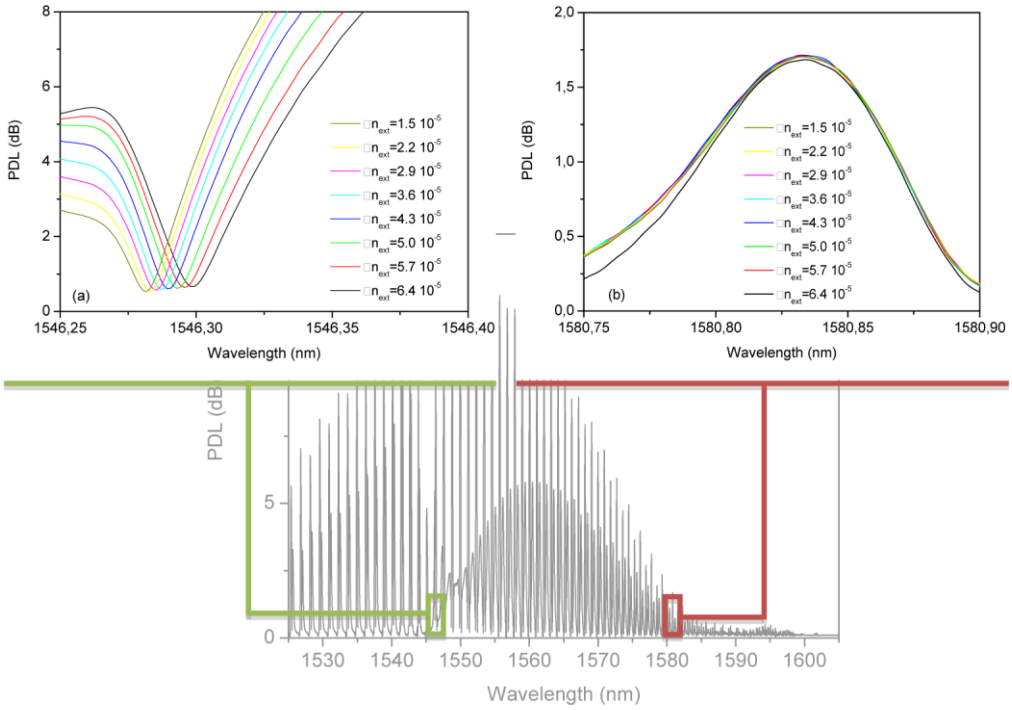

Fig. 6. PDL curves for some SRI values around 1.34. Left: zoom on a downward peak close to the SPR signature. Right: zoom on a peak around 1580 nm.

#139453 - $15.00 USD Received 9 Dec 2010; revised 10 Jan 2011; accepted 10 Jan 2011; published 13 Jan 2011

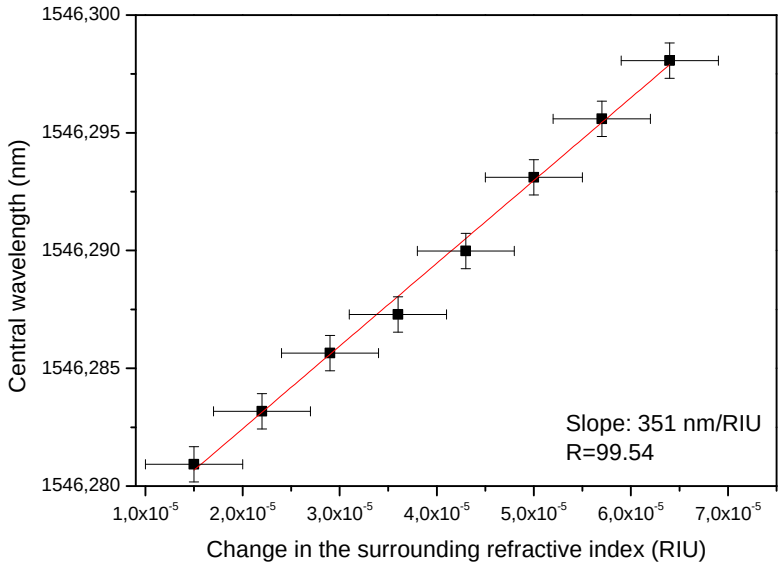

Fig. 7. SPR wavelength shift as a function of the SRI.

Repeatability tests have also been conducted on series of 50 measurements taken in the same operating conditions for some specific refractive index values between 1.31 and 1.38. As an example, Fig. 8 shows a histogram that represents the results obtained in terms of the detection of the resonance wavelength for an SRI kept constant around 1.34. A Gaussian-shaped distribution with standard deviation of 3 pm is obtained, yielding a sensor resolution slightly better than 1 10^{-5} [13]. In practice, the main source of error remains the temperature fluctuations (a variation of 0.1 °C induces a change of the SRI of about 1 10^{-5}).

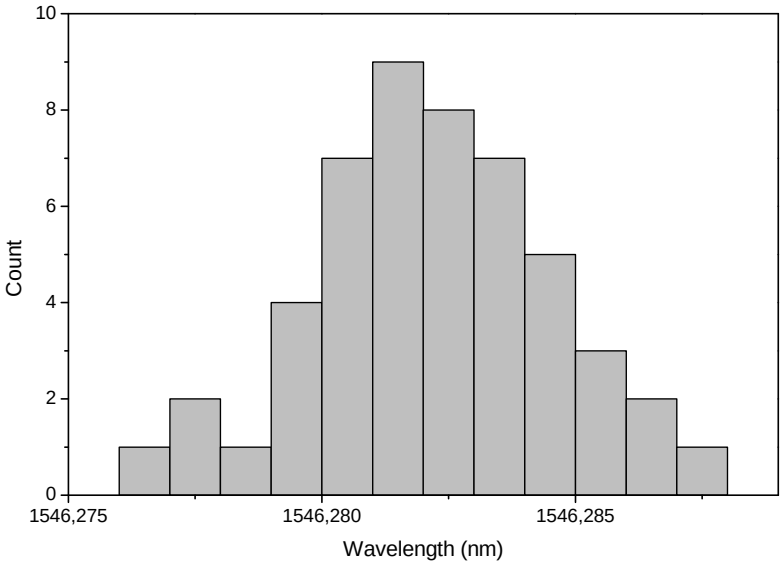

Fig. 8. Histogram resulting from the repeatability test.

Finally, the robustness over polarization instabilities has also been evaluated. Basically, the connecting fibers were moved during the measurements. As the optical vector analyzer

#139453 - $15.00 USD Received 9 Dec 2010; revised 10 Jan 2011; accepted 10 Jan 2011; published 13 Jan 2011

presents its own internal reference, the Jones matrix computation was not modified by a normal fiber handling, which in turn does not affect the proposed demodulation technique and yields results similar to those reported in Fig. 8. Hence, contrary to other techniques reported so far, working with the Jones matrix is compatible with real time operation (a complete measurement in a 80 nm window takes a few seconds) and does not require a tight control of the input SOP.

4. Conclusion

In this work, we have demonstrated the operating principle of a new demodulation technique applied to plasmonic fiber grating sensors using gold-coated TFBGs. The proposed technique exploits the information contained in the Jones matrix associated to the TFBG transmitted signal. In particular, the PDL and s_1 evolutions with wavelength obtained from the Jones matrix contain an ambiguous signature of the SPR that can be readily tracked as a function of the SRI. Unlike previously reported methods, our technique is robust over polarization instabilities and can work with real time operating systems. Using spectral features with 10^5 finesse in the PDL spectrum near the SPR resonance, we further demonstrated an improved sensing accuracy as the maximum error on the computation of the SRI has been measured to be equal to ~1 10^{-5} RIU, which is suited for practical application in biosensing.

Acknowledgment

Christophe Caucheteur is supported by the Fonds National de la Recherche Scientifique (F.R.S.-FNRS). Li-Yang Shao thanks the National Natural Science Foundation of China under grant N° 61007050. Jacques Albert holds the Canada Research Chair in Advanced Photonic Components at Carleton University and this research is funded by NSERC and LxData. The authors acknowledge the Attraction Pole Program IAP 6/10 of the BelSPo and the Opti2Mat project. They are indebted to Dr Marc Debliquy for his help during the experiments.

#139453 - $15.00 USD Received 9 Dec 2010; revised 10 Jan 2011; accepted 10 Jan 2011; published 13 Jan 2011